J MATER RES TECHNOL. 2017;6(3):297–301

Available online at www.sciencedirect.com

jmr&t Journal of Materials Research and Technology

www.jmrt.com.br

Short Communication

Preparation and luminescence of a new violet blue phosphor derived from proton-type zirconium phosphate

Susumu Nakayama[a,*], *Masatomi Sakamoto*[b]

[a] *Department of Applied Chemistry and Biotechnology, National Institute of Technology, Niihama College, Niihama-shi, Japan*
[b] *Material and Biological Chemistry, Graduate School of Science and Engineering, Yamagata University, Yamagata-shi, Japan*

ARTICLE INFO

Article history:
Received 15 September 2016
Accepted 29 March 2017
Available online 25 May 2017

Keywords:
Ceramics
Chemical synthesis
Heat treatment
Photoluminescence
Defects

ABSTRACT

A violet blue phosphor was prepared by thermal treatment of $HZr_2(PO_4)_3$ at 700 °C in a reducing atmosphere and its PL was investigated. The phosphor shows violet blue emissions at around 392 nm when excited by 254 nm UV light. Its absorptivity, internal and external quantum efficiency are found to be 43, 41, and 18%, respectively, at room temperature when excited at 254 nm. Analyses using non-dispersive infrared absorption, X-ray fluorescence, scanning electron microscopy, X-ray photoelectron spectroscopy, and X-ray diffraction suggest that such an emission originates from the formation of hydrogen and oxygen vacancies in the phosphor during the thermal treatment of $HZr_2(PO_4)_3$.

1. Introduction

Hydrogen gas has been widely used as one of the deoxidizing agents to develop various metal oxides with oxygen vacancies and of particular interest is its application for the fabrication of a green phosphor, ZnO [1–5]. Such phosphors, which do not contain light-emitting metal elements (extrinsic activators: Eu, Tb, Tm, etc.), have attracted great attention in respect different from $Zn_2SiO_4:Eu^{3+}$, $Ca_{12}Al_{14}O_{32}Cl_2:Tb^{3+}$, and $Gd_4O_3F_6:RE^{3+}$ (RE = Yb, Er, Ho and Tm) phosphors [6–8]. These studies have inspired us to investigate whether zirconium phosphates including $HZr_2(PO_4)_3$ will form oxygen and hydrogen vacancies. The proton-type zirconium phosphate $HZr_2(PO_4)_3$, which features a Nasicon-type (NZP, $NaZr_2(PO_4)_3$) crystal structure with rhombohedral symmetry consisting of a three-dimensional rigid framework with corner linked ZrO_6 octahedra and PO_4 tetrahedra, has been known to be an effective ion exchanger and to possess high resistance to heat, chemicals, radiation, corrosion, and mechanical shock [9,10]. Fig. 1(a) shows the crystal structure proposed for $HZr_2(PO_4)_3$. Preliminary experiments revealed that $HZr_2(PO_4)_3$ powders

* *Corresponding author.*
E-mail: nakayama@chem.niihama-nct.ac.jp (S. Nakayama).
http://dx.doi.org/10.1016/j.jmrt.2017.03.001

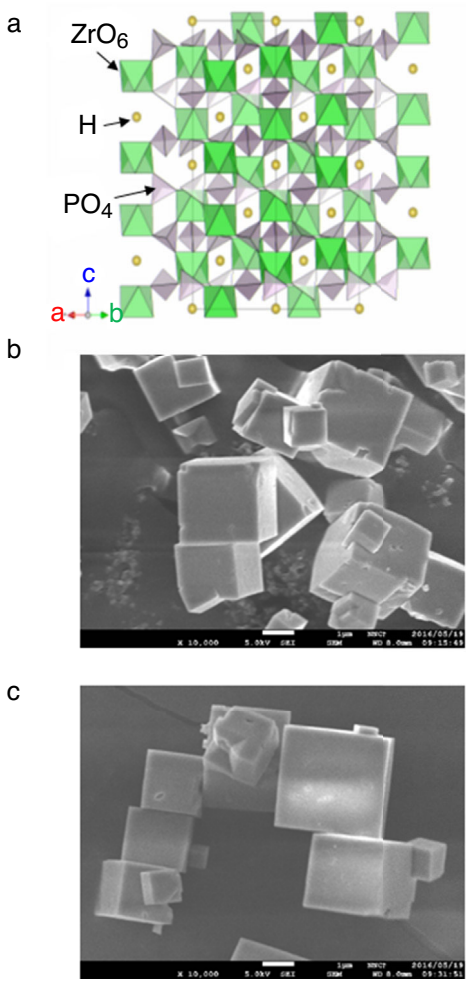

Fig. 1 – Crystal structure proposed for HZP (a); SEM micrographs of HZP (b) and HZP-r (c).

contain such vacancies and can act as a bright phosphor as expected. The fluorescence was a violet emission at around 392 nm under 254 nm excitation. So far, SiO_2—GeO_2 amorphous films, which contain oxygen vacancies, are known to show a bright PL of violet color [11,12]. In addition, ZrO_2:Ti,P blue phosphor, which also consists of oxygen vacancies, has been reported [13]. On the other hand, Ce^{3+}-doped Gd_2SiO_5 [14] and Ce^{3+}-doped $BaZrSi_2O_9$ [15] are well-known as very bright violet or blue phosphors, which contain extrinsic activators. The proton-type zirconium phosphate presented here is a new type of violet blue phosphor, which has not been reported yet. This kind of phosphor is worth studying for the following reasons: (1) it does not contain extrinsic activators, (2) it is easy to synthesize, (3) it has the potential to outperform existing materials, and (4) it is expected to possess interesting luminescence properties. In this work, more detailed PL properties of this new type of violet blue phosphor are investigated.

2. Experimental

Crystalline powders of proton-type zirconium phosphate, $HZr_2(PO_4)_3$ (hereafter abbreviated as HZP), were prepared by thermal decomposition of $NH_4Zr_2(PO_4)_3$ at 700 °C for 2 h in air. The as-prepared HZP powder was thermally treated at 700 °C for 2 h in a 300 mL min^{-1} 3%-H_2 (N_2 balance) gas flow to obtain a violet phosphor (here after abbreviated as HZP-r). $NH_4Zr_2(PO_4)_3$ was synthesized as follows. The precipitate was prepared by a hydrothermal reaction at 95 °C for 72 h from a solution containing 200 cm^3 of 0.41 mol dm^{-3}-$ZrOCl_2{\cdot}8H_2O$, 300 cm^3 of 0.47 mol dm^{-3}-$H_2C_2O_4{\cdot}2H_2O$, and 100 cm^3 of 1.09 mol dm^{-3}-$NH_4H_2PO_4$ adjusted to pH 4.5 by 3 mol dm^{-3} NH_3 aqueous ammonia. The precipitate obtained was filtered and dried at 250 °C for 24 h.

Elemental analyses of H and O were carried out by means of the inert gas melt/non-dispersive infrared (NDIR) method using a simultaneous oxygen/nitrogen/hydrogen analyzer EMGA-930 (HORIBA Ltd.). Contents of Zr and P were determined with an X-ray fluorescence (XRF) spectrometer Simultix 14 (Rigaku Co.).

The obtained violet phosphor was characterized by scanning electron microscopy (SEM) observation, X-ray photoelectron spectroscopy (XPS), X-ray diffraction (XRD), and fluorescence spectroscopy. The crystal morphology was observed using a field emission SEM with a semi-in-lens JSM-7500F (JEOL Ltd.) at 5 kV. XPS analyses for the electronic states of P2*p* were carried out with X-ray photoelectron spectroscopy on a Quantera SXM (Physical Electronics, Inc.). An Al-Kα monochromatized radiation (50 W) was employed as X-ray source. The X-ray beam size was a 100 $\mu m\phi$. XRD data were obtained using an X-ray diffractometer MiniFlex II (Rigaku Co.) with CuKα_1 radiation ($\lambda = 0.154$ nm) and a graphite monochromator. The X-ray generator worked at 30 kV and 15 mA. The scans were performed for 15 min within the 2θ range of 10–40° using a scan step of $(2\theta) = 0.005°$. Excitation and emission spectra were measured on a spectrofluorometer FP-6500 (JASCO Co.) with a scan rate of 500 nm min^{-1} and a step size of 0.1 nm using a 150 W ozone-free Xenon lamp. Quantum efficiency was determined with a Quantaurus-QY absolute PL quantum yield spectrometer C11347-01 (Hamamatsu Photonics K.K.) at an excitation wavelength of 254 nm. The absorptivity (*A*) was calculated according to the following expression.

$$\text{Absorptivity} = \frac{\{1 - (\text{excitation light intensity with sample})\}}{(\text{excitation light intensity without sample})}$$

The internal quantum efficiency was measured using an integrating sphere attached to a multi-channel CCD detector and a Xenon lamp as excitation source. The external quantum efficiency was calculated by multiplying absorptivity and internal quantum efficiency. The PL lifetime was measured using a Quantaurus-τ fluorescence lifetime spectrometer C11367-24 (Hamamatsu Photonics K.K.) at an excitation wavelength of 280 nm and an emission wavelength of 392 nm. Measurements except for the determination of the internal quantum efficiency were conducted at room temperature (RT).

3. Results and discussion

Element analysis using NDIR and XRF of HZP (starting material of HZP-r) reveals an elemental distribution of 0.31, 38.07, 20.97, and 41.59 wt%, whereas HZP-r (sample prepared by the thermal treatment of HZP in 3%-H_2 atmosphere) contains 0.17,

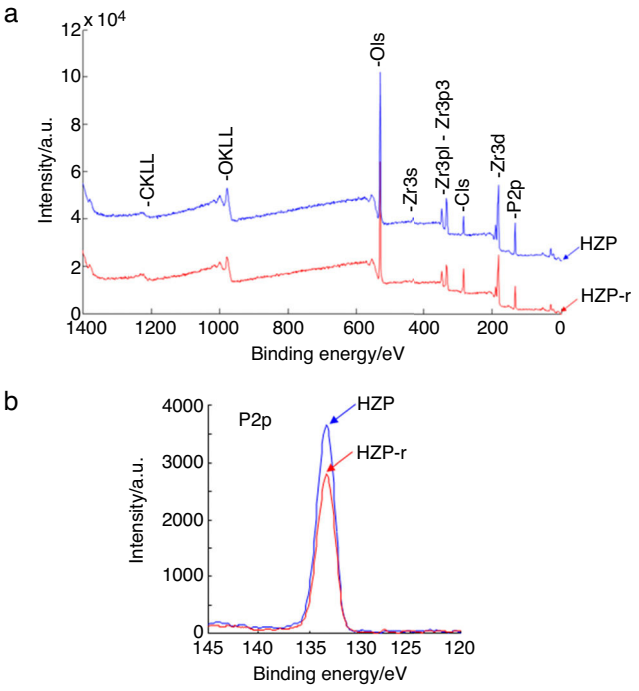

Fig. 2 – XPS wide spectra (a) and P2p XPS spectra (b) of HZP and HZP-r.

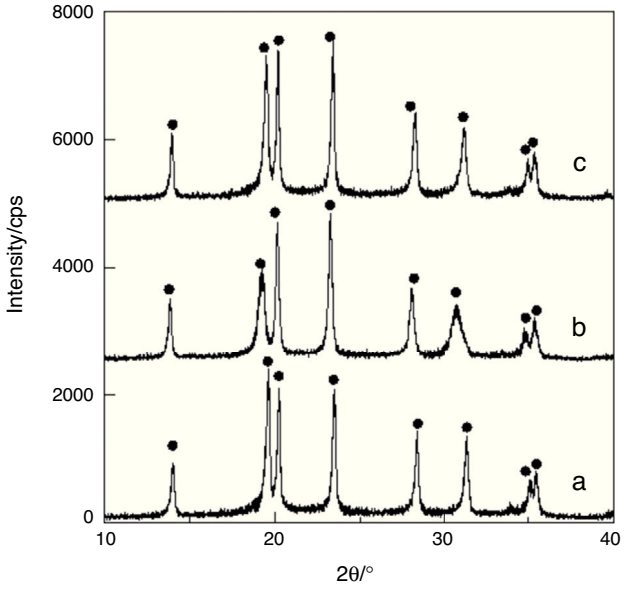

Fig. 3 – X-ray powder diffraction patterns of HZP-r (a), starting material HZP (b), and a sample prepared by thermal treatment of HZP-r (c). Closed circles represent peak data of $HZr_2(PO_4)_3$ reported in ICDD No. 38-4.

38.72, 21.17, and 40.37 wt% of H, Zr, P, and O, respectively. Assuming that the number of Zr atoms is 2, the chemical composition of HZP can be estimated to be $H_{1.47}Zr_2P_{3.24}O_{12.47}$ for HZP, suggesting $HZr_2(PO_4)_3$ and $(H_3O)Zr_2(PO_4)_3$ exist in a molar ratio of 0.76:0.24 as major components along with a small amount of P_2O_5. In relation to this, we previously reported that $HZr_2(PO_4)_3$ absorbs moisture from ambient air to form $(H_3O)Zr_2(PO_4)_3$, which reverts to $HZr_2(PO_4)_3$ at 205 °C [16]. As for HZP-r, its chemical composition can be calculated to be $H_{0.80}Zr_2P_{3.22}O_{11.90}$, suggesting the formation of hydrogen and oxygen vacancies during thermal treatment of HZP at 700 °C in 3% H_2.

The SEM micrographs of HZP and HZP-r are shown in Fig. 1(b) and (c), respectively. The crystal morphology of HZP and HZP-r is cubic with a side length of approximately 1–3 μm. Furthermore, no change in crystal morphology induced by H_2 reduction can be observed.

Fig. 2(a) shows the XPS wide spectra of HZP and HZP-r. In these two spectra, peaks attributable to C, O, Zr, and P are observed. Among these detected elements, the P2p XPS spectra were further evaluated in order to investigate the valence state of P (Fig. 2(b)). The P2p peaks for HZP and HZP-r are observed at almost identical binding energies of around 133.4 eV and their peak shapes are also similar, suggesting no significant difference in the electronic state of P between HZP and HZP-r. It is presumed that the valence of the P atoms in HZP and HZP-r is +5.

Fig. 3 shows the X-ray powder diffraction patterns of HZP-r, HZP, and a sample prepared by thermal treatment of HZP-r at 700 °C for 2 h in air. All three XRD patterns are in good agreement with those found in the corresponding ICDD files ((38-4, $HZr_2(PO_4)_3$, hexagonal, R-3c) and (38–67, $(H_3O)Zr_2(PO_4)_3$, hexagonal, R-3c)). The lattice parameters and unit cell volume of HZP-r are $a = 0.876$ nm, $c = 2.249$ nm, and 1.495 nm^3, respectively. These values are smaller than those of HZP ($a = 0.879$ nm, $c = 2.319$ nm, cell volume = 1.552 nm^3), probably due to the formation of hydrogen and oxygen vacancies in HZP-r induced by H_2 reduction of HZP. Lattice parameters and unit cell volume for the sample prepared by thermal treatment of HZP-r at 700 °C for 2 h in air are estimated to be $a = 0.879$ nm, $c = 2.261$ nm, and 1.514 nm^3, respectively, suggesting that the oxygen vacancies were, to some extent, removed during thermal treatment in air as partial oxidation of HZP-r occurred.

Excitation and emission spectra of HZP-r are shown in Fig. 4. HZP-r can be efficiently excited by UV light of 254 nm, yielding a violet blue emission at around 392 nm. The CIE (x, y) was calculated as (x, y) = (0.188, 0.140). Thus, the HZP-r emission is exactly on the violet blue light emitting area under 254 nm excitation, indicating that the HZP-r is a violet blue phosphor. Absorptivity, internal and external quantum efficiency of the phosphor, HZP-r, at the excitation wavelength of 254 nm are 43, 41, and 18%, respectively. As a comparison, the internal quantum efficiency of Ce^{3+}-doped $BaZrSi_2O_9$ phosphor, which has a very bright PL at around 432–451 nm, was 92.3% under 340 nm excitation [15], about double the value of HZP-r. In contrast to HZP-r, HZP exhibited no violet blue emission, and no significant emission was observed for the sample prepared by thermal treatment of HZP-r at 700 °C in air. These different observations suggest that there is a threshold concentration of hydrogen and/or oxygen vacancies above which the emission can be clearly observed. It is plausible that the strong violet blue emission of HZP-r is caused by its hydrogen and oxygen vacancies; elucidation of the emission mechanisms is in progress. In Fig. 4, the PL decay profile of the phosphor, HZP-r is inserted. It is assumed that the decay

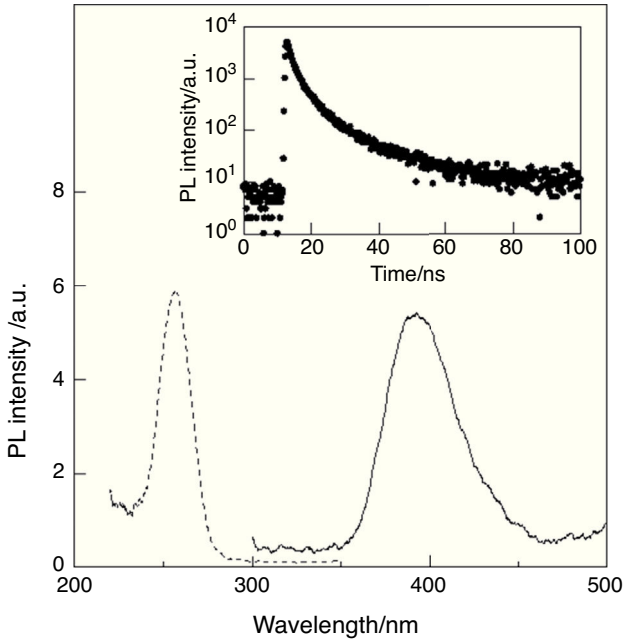

Fig. 4 – Excitation (left, emission: 392 nm) and emission (right, excitation: 254 nm) spectra of HZP-r at room temperature. The inset is the PL decay profile at 392 nm of HZP-r at room temperature (excitation wavelength: 280 nm).

is non-exponential and the average PL lifetime was estimated to be 6.4 ns. We believe that the non-exponential decay originates from a continuous distribution of lifetimes due to an inhomogeneity of the PL centers or some exotic recombination processes, such as tunneling recombination.

The temperature dependence of the internal quantum efficiency of the phosphor, HZP-r, was investigated in the range between 25 and 163 °C. Temperature quenching is generally observed in phosphors; however, a temperature rise of a device using the phosphors as a constituent material is inevitable due to heat radiation from the high power light emitting diode (LED) and the backlight of the liquid crystal display (LCD). Therefore, phosphors featuring suppressed temperature quenching are required. As shown in Fig. 5, the efficiency decreases linearly with a rise in temperature and is found to be 20% at 163 °C, which is about half of that obtained at 25 °C. For comparison, the measured PL intensity of Ce^{3+}-doped $BaZrSi_2O_9$ phosphor at 123 °C retained 44.6% of the value measured at room temperature [15], which is nearly equal to that of HZP-r.

4. Conclusions

A new type of violet blue phosphor, $H_{0.80}Zr_2P_{3.22}O_{11.90}$, was prepared by thermal treatment of proton-type zirconium phosphate, $HZr_2(PO_4)_3$, at 700 °C in 3%-H_2 atmosphere and its PL was investigated. No change in crystal morphology of proton-type zirconium phosphate induced by H_2 thermal treatment was observed. The internal quantum efficiency of the violet blue phosphor at the excitation wavelength of 254 nm was 41%. The type of PL decay of $H_{0.80}Zr_2P_{3.22}O_{11.90}$

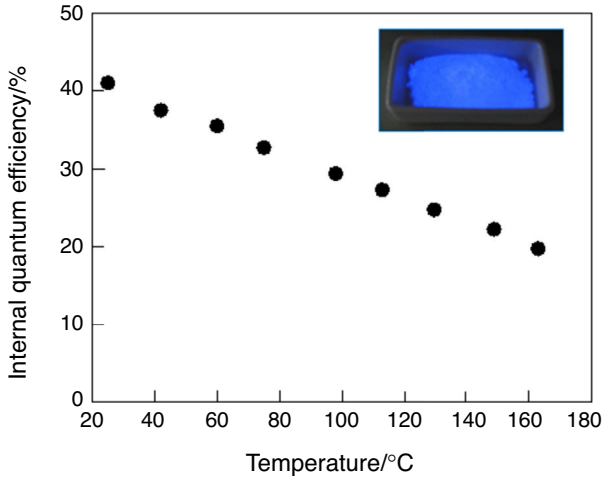

Fig. 5 – Temperature dependence of the internal quantum efficiency of HZP-r. The excitation wavelength is 254 nm. The inset shows a digital photograph of HZP-r irradiated under 254 nm UV light at room temperature.

was found to be non-exponential and the average PL lifetime was about 6.4 ns. The PL intensity decreased linearly with increasing temperature (163 °C) retaining about 50% of the value measured at 25 °C. It is plausible that the emission is due to the hydrogen and oxygen vacancies in the phosphor. Research on H_2 treatment conditions and hydrogen/oxygen defects observations are in progress in order to further investigate the PL mechanisms.

Conflicts of interest

The authors declare no conflicts of interest.

Acknowledgements

We would like to thank Hamamatsu Photonics K.K. for the measurements of quantum efficiency and PL lifetime, HORIBA Ltd. for the elemental analyses of H, and Editage (www.editage.jp) for help with English language editing.

REFERENCES

[1] Vanheusden K, Warren WL, Seager CH, Tallant DR, Voigt JA. Mechanisms behind green photoluminescence in ZnO phosphor powders. J Appl Phys 1996;79:7983–90, http://dx.doi.org/10.1063/1.362349.

[2] Mishra AK, Chaudhuri SK, Mukherjee S, Priyam A, Saha A, Dasa D. Characterization of defects in ZnO nanocrystals: photoluminescence and positron annihilation spectroscopic studies. J Appl Phys 2007;102:103514, http://dx.doi.org/10.1063/1.2817598.

[3] Ohashi N, Wang YG, Ishigaki T, Wada Y, Taguchi H, Sakaguchi I, et al. Lowered stimulated emission threshold of zinc oxide by hydrogen doping with pulsed argon–hydrogen plasma. J Cryst Growth 2007;306:316–20, http://dx.doi.org/10.1016/j.jcrysgro.2007.05.024.

[4] Shi Q, Wang Z, Liu Y, Yang B, Wang G, Wang W, et al. Single-phased emission-tunable Mg-doped ZnO phosphors for white LEDs. J Alloys Compd 2013;553:172–6, http://dx.doi.org/10.1016/j.jallcom.2012.11.135.

[5] Li C, Lv J, Liang Z, Yao S. Study on the optical absorption and green emission of ZnO phosphors by varying Al doping contents. Opt Mater 2013;35:586–9, http://dx.doi.org/10.1016/j.optmat.2012.10.037.

[6] Omar NAS, Fen YW, Matori KA. Europium doped low cost Zn_2SiO_4 based glass ceramics: a study on fabrication, structural, energy band gap and luminescence properties. Mater Sci Semi Proc 2016;61:27–34, http://dx.doi.org/10.1016/j.mssp.2016.12.040.

[7] Chen Y, Wang X, Bao Y. Study on a new green phosphor $Ca_{12}Al_{14}O_{32}Cl_2$: Tb^{3+} derived from Tb-doped Ca–Al layered double hydroxide. Cur Appl Phys 2017;17:78–84, http://dx.doi.org/10.1016/j.cap.2016.11.003.

[8] Zhang J, Jia J. Morphologies and up-conversion luminescence of $Gd_4O_3F_6$:RE^{3+} (RE = Yb, Er, Ho and Tm) phosphors by hydrothermal synthesis. J Lumin 2016;174:1–5, http://dx.doi.org/10.1016/j.jlumin.2016.01.030.

[9] Vesely V, Pekarek V. Synthetic inorganic ion-exchangers – I: Hydrous oxides and acidic salts of multivalent metals. Talanta 1972;19:219–62.

[10] Scheetz BE, Agrawal DK, Breval E, Roy R. Sodium zirconium phosphate (NZP) as a host structure for nuclear waste immobilizaition: a review. Waste Manage 1994;14:489–505.

[11] Arai N, Tsuji H, Hattori M, Ohsaki M, Kotaki H, Ishibashi T, et al. Luminescence properties of Ge implanted SiO_2:Ge and GeO_2:Ge films. Appl Surf Sci 2009;256:954–7, http://dx.doi.org/10.1016/j.apsusc.2009.05.062.

[12] Trukhin AN. Luminescence of polymorph crystalline and glassy SiO_2, GeO_2. J Non-Cryst Solids 2009;355:1013–9, http://dx.doi.org/10.1016/j.jnoncrysol.2009.01.040.

[13] Nakayama S, Sakamoto M. Fluorescence property of ZrO_2:Ti phosphor and its enhancement in fluorescent intensity by adding phosphorus. J Mater Res Technol 2016;5:289–92, http://dx.doi.org/10.1016/j.jmrt.2016.03.005.

[14] Parganiha Y, Kaur J, Dubey V, Shrivastava R, Chandrakar D. Violet blue emission and thermoluminescence glow curve analysis of Gd_2SiO_5:Ce^{3+} phosphor. Optik 2016;127:6243–52, http://dx.doi.org/10.1016/j.ijleo.2016.04.064.

[15] Liu S, Liang Y, Zhu Y, Wu X, Xu R, Tong M, et al. Synthesis and luminescence properties of novel Ce^{3+} doped $BaZrSi_3O_9$ phosphors. Opt Laser Technol 2016;84:1–8, http://dx.doi.org/10.1016/j.optlastec.2016.04.010.

[16] Hashimoto C, Nakayama S. Effect of treatment temperature on the immobilization of Cs and Sr to $HZr_2(PO_4)_3$ using an autoclave. J Nucl Mater 2013;440:153–7, http://dx.doi.org/10.1016/j.jnucmat.2013.04.085.